International Journal of Mechanical Sciences 151 (2019) 95–105

Contents lists available at ScienceDirect

International Journal of Mechanical Sciences

journal homepage: www.elsevier.com/locate/ijmecsci

Transient cooling characteristics of Al_2O_3-water nanofluid flow in a microchannel subject to a sudden-pulsed heat flux

C.J. Ho[a,*], Yu-Hui Chiou[a], Wei-Mon Yan[b,c,*], Mohammad Ghalambaz[d]

[a] Department of Mechanical Engineering, National Cheng-Kung University, Tainan 70101, Taiwan
[b] Department of Energy and Refrigerating Air-Conditioning Engineering, National Taipei University of Technology, Taipei 10608, Taiwan
[c] Research Center of Energy Conservation for New Generation of Residential, Commercial, and Industrial Sectors, National Taipei University of Technology, Taipei 10608, Taiwan
[d] Department of Mechanical Engineering, Dezful Branch, Islamic Azad University, Dezful, Iran

ARTICLE INFO

Keywords:
Al2O3 water nanofluid
Phase change material
Unsteady heat transfer
Minichannel

ABSTRACT

Transient cooling characteristics of Al_2O_3-water nanofluid flow in a microchannel subject to sudden-pulsed heat flux are numerically examined in details. The attention is focused on the effects of microencapsulated phase change material (MEPCM) inside top wall of a microchannel on the transient cooling heat transfer behaviour of the microchannel. Two small portion of the bottom channel wall are exposed to a pulse heat flux. The Al_2O_3-water nanofluid as the working fluid with a fully developed velocity profile flows into the microchannel to cool the channel walls. Transient conjugate heat transfer is studied using a three-dimensional model in the three parts of the microchannel which are the nanofluid flow, the solid walls of the channel, and the MEPCM layer. The partial differential equations governing the energy conservation are presented and transformed into a dimensionless form. The finite volume method is employed to numerically integrate the equations for the temperature distribution in the microchannel. The numerical results are compared with the available works in the literature and found in good agreement. Besides, the predictions show that the presence of the MEPCM layer cannot effectively control the rise of the temperature of the microchannel in the presence of a pulse heat flux. For a typical pulse heat flux, the bulk temperature of the channel can be raised up to 2 °C while the presence of the MEPCM layer would only suppress the temperature rise by 0.2 °C. It is also found that the temperature of the top wall is under the significant influence of the MEPCM layer. The increase of the amplitude of the heat flux pulse results in better cooling effect of the MEPCM layer.

1. Introduction

The heat removal has become important issue in further miniaturization of microelectronics, due to the significant grow of the integration density and waste-heat generation of micro-chipsets, processors and high-power density transformers. Developing high performance heat removal systems are playing a key role in advancement of power electronic devices. These devices produce notable amount of heat due to their increased heat current-voltage handling-capability. Removing a significant amount of waste-heat from a constrained small space of the component requires sophisticated cooling systems and new advanced techniques [1]. There are also many other industrial processes such as aircrafts, and avionics systems, and petrochemical plants, that they require efficient cooling systems.

The experimental researches reveal that micro-channel heat sinks are capable of removing high surface heat fluxes in the order of 10^4 W/m^2 and higher with a reasonable temperature difference [2, 3]. The microchannels are also capable of providing a thermal resistance as low as 0.03 °C/W [4]. As indicated by Vafai and Zhu [1], one disadvantage of microchannel heat-sinks is the comparatively high temperature growth along the channel due to low flow rate of coolant and the large amount of the surface heat-flux that should be removed. In some applications such as cooling of electrical components, a significant temperature difference among the heat sink is extremely undesirable as it produces thermal stresses in the component. This thermal stress is due to the difference in the thermal expansion behaviour of the structure materials of the component. Moreover, the temperature raise and the temperature difference in an electronic component induce undesirable influence on the electrical performance of the component [1]. Moreover, in some electronic or industrial applications, there are situations in which the high power active time of the electronic component is limited or periodic. Hence, the generated waste-heat in the component can be seen is in the form of a pulse heat flux. Such a pulse heat flux can increase

* Corresponding authors.
E-mail addresses: cjho@mail.ncku.edu.tw (C.J. Ho), wmyan@ntut.edu.tw (W.-M. Yan).

https://doi.org/10.1016/j.ijmecsci.2018.11.017
Received 8 October 2018; Received in revised form 13 November 2018; Accepted 18 November 2018
Available online 19 November 2018

Nomenclature

A	Perimeter area for MEPCM particles (m^2)
A^+	Area (m^2)
$AR_{bw,x}$	Aspect ratio of the bottom wall
$AR_{ch,x}$	Aspect ratio of the channel wall
$AR_{cw,x}$	Aspect ratio of the top wall
$\dot{Q}$	Flow rate (m^3/s)
$\Delta T_{ref,bf}$	Reference temperature difference
c_p	Specific heat at constant pressure
d^+	Average particle size
D^+_h	Hydraulic diameter
H	Dimensionless height
h	Heat transfer coefficient (W/m•K)
H^+	Height (m)
h_{ls}	Solid-liquid phase change latent heat (J/kg)
k	Conductive thermal coefficient (W/m^2•K)
L^+	The channel length
n	Surface normal vector
Nu	Nusselt number
P	Heat flux pulse duration
p	Pressure (kPa)
Pe	Peclet number
Pr	Prandtl number
q	Heat transfer (W)
$q"$	Heat flux (W/m^2)
R	Thermal resistance
Re	Reynolds number
Sb^*	Correct secondary cooling parameters
Ste^*	Stefan number
T	Temperature (°C)
t	Time (s)
T_M	Fusion temperature (°C)
u^+	Fluid velocity
$u^+_{x,fd}$	Inlet fluid velocity (m/s)
U	Interstitial overall heat transfer coefficient
V	MEPCM particle volume
W	Dimensionless width
W^+	Width
x^+	x direction coordinates
y^+	y direction coordinates
z^+	z direction coordinates

Greek symbol

α	Thermal diffusivity (m^2/s)
β	Coefficient of thermal expansion (1/K)
γ	Heat flux pulse amplitude
ϵ	Ratio of comparison and MEPCM porosity
θ	Dimensionless temperature
μ	Dynamic viscosity (N•s/m^2)
ξ	Melting rate
ρ	Density (kg/m^3)
υ	Kinematic viscosity (m^2/s)
ϕ	Nanoparticles
ω	Mass fraction of nanoparticles

Subscript symbol

air	Air between the MEPCM particles
b	Bulk (average) properties
bf	Base fluid
bf/nf	Base fluid to nanofluid ratio
bw	Bottom wall solid
ch	Channel
ch,b	The interface between the flow in channel and bottom wall
ch,s	The interface between the flow in channel and side wall
ch,t	The interface between the flow in channel and top wall
cond	Conduction
cw	Top wall
d	Outlet adiabatic section
h1	First heating section
h2	Second heating section
i	Inner wall
in	Inlet
int	Internal
max	Maximum
nf	Nanofluid
np	Nanoparticle
o	Outer wall
pcml	Phase change microcapsule layer
pcmp	Microencapsulated particle
sw	Side wall
w	Wall surface
x	x direction
y	y direction
z	z direction

Super scripts

*	ratio
+	Dimensional parameter

the temperature difference along a microchannel for a period of time accordingly. Thus, the methods that are capable of reducing the temperature difference along a microchannel and managing the pulse heat fluxes are highly demanded.

Many various aspects of flow and heat transfer in a channel have been investigated by recent researchers. The effect of using a perforated baffle in a channel [5], a channel with a rotating inner surface [6], magnetic field effects [7] have been addressed in the recent year. One of the new aspects of enhancing the cooling performance of a channel is using nanofluids as the working fluid.

Nanofluids are a new type of engineered working fluids, which are a stable suspension of nanoparticles and a base fluid. Nanofluids show enhanced thermophysical and thermal properties compared to the pure base fluid. Thus, nanofluids are proposed as alternative working fluids in many cooling systems. Shirvan et al. [8] have utilized alumina nanoparticles to enhance the heat transfer of the working fluid in a channel. There are excellent comprehensive studies that reviewed the preparation [9], applications [10-12] and thermophysical properties of nanofluids [13].

Ho and his colleagues [3, 15, 15] as well as Farid and Hallaj [16] have proposed using a particulate suspension of liquid/solid phase change material as a working fluid to regulate the temperature differences along a microchannel. Results of [14] disclose that a coolant containing MEPCM shows better heat transfer performance compared to a regular coolant. In addition, employing a coolant with MEPCM as the working fluid results in a lower wall temperature of microchannel. There are also interesting studies that addressed the effect of using phase change materials in thermal systems such as the melting process of erythritol in spheres [17], melting in a square cavity [18], melting of a nano-enhanced phase change material using nanoparticles [19, 20], and hybrid nanoparticles [21]. In [22], a new fundamental design of a microchannel is proposed in which a layer of phase change material is placed in the channel walls to enhance the surface heat absorption capacity of the microchannel structure. Jamekhorshid et al. [23] have performed an excellent review on the microencapsulated phase change materials and their applications in thermal energy storage systems. Furthermore, Sabbah et al. [24] have theoretically investigated the effect

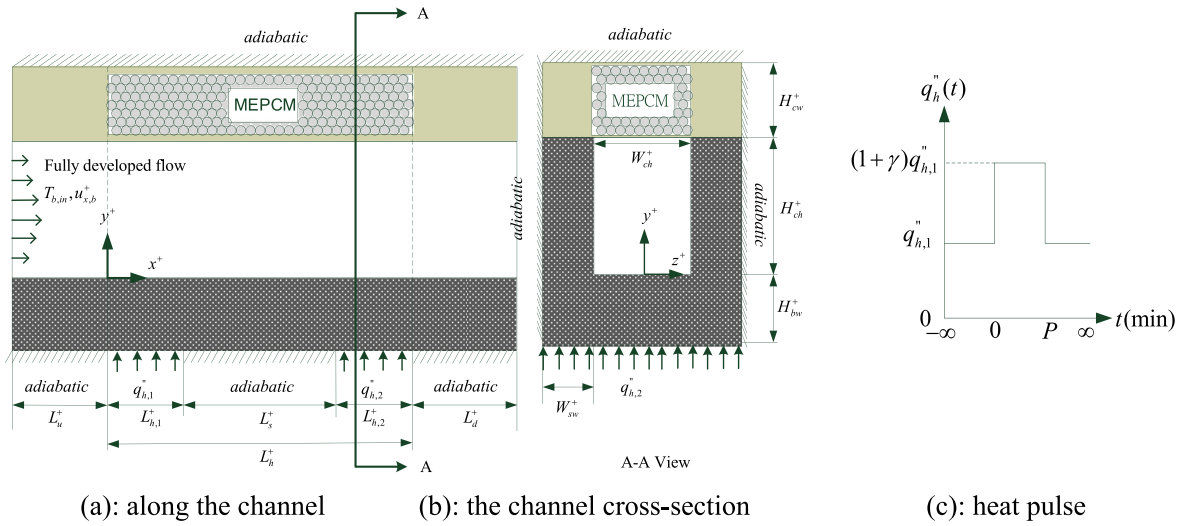

(a): along the channel (b): the channel cross-section (c): heat pulse

Fig. 1. The schematic view of the microchannel physical model and MEPCM in celling wall; (a) the side view in flow direction, (b) the cross-section view, (c) the heat flux pulse at the heated zones.

of using PCMs on the thermal management of high-power lithium-ion packs. They compared the effect of using PCMs with an air-cooled system. They found that a system using PCMs is capable of safe operation in stressful conditions and acts better than an air-cooled system. Considering high-temperature environment (40 °C), Ping et al. [25] have addressed the effect of using PCM-fins for thermal management of Li-ion battery module. The PCM-fins are utilized to diminish the extreme pick temperatures and enhance the temperature-uniformity of the battery module. The results of this study demonstrated that PCM-fin structure is capable of reducing failure-risk of batteries by enhancing the heat dissipation efficiency in passive thermal-management systems. Samimi et al. [26] have tried to enhance the low thermal conductivity of PCMs using carbon fibers for application in Li-ion battery cells. The outcomes indicate that using carbon fibers in the PCM would enhance the performance of Li-ion battery cell.

In [22], a Chinese company has introduced a patent to enhance the surface heat absorption capacity of the microchannel and improve the temperature control capability of the channel. Following the idea of [22], the present study aims to model and simulate three-dimensional transient heat transfer of Al_2O_3-water nanofluids in a microchannel in which there is a layer of microencapsulated phase change material embedded inside the top wall of the channel, and the bottom wall of the channel is subject to a pulse heat flux. To the best of the author's knowledge, the results of the present study are new and have not been addressed yet.

2. Analysis

2.1. Model description

The schematic view of the physical model of the microchannel and the coordinate system are illustrated in Fig. 1. The microchannel section is rectangular and the walls of the channel are thick. The solid walls are highly thermal conductive made of copper. The geometrical and physical details of the channel are represented in Figs 1(a) and (b). All of the outer walls of the channel are well insulated and can be considered as adiabatic. Two wall heat flux sources of $q''_{h,1} = q''_{h,2} = q''_h$ are imposed at the bottom of the channel.

In most of electronic devices or computer chipsets, the rate of the electrical power demand of the device is known for performing a computational task. This electrical demand later would be changed into the heat loss and should be removed from the surface of the chip. Hence, the heat flux is considered as the key boundary condition of the present study. The characteristic parameters of the study are the temperature profiles in the channel and at the location of heat pulses which show the surface temperature of the chipset. The elements are subject to transient heat flux with the pulse time P and amplitude of γ. As plotted in Fig. 1(c), the wall heat flux suddenly rises from its base flux of $q''_{h,1}$ to $(1+\gamma)q''_{h,1}$ during a pulse time of P, and then, it drops to its base flux of $q''_{h,1}$. A fully developed Al_2O_3-water nanofluid as working fluid enters the channel with the uniform temperature of T_i. The fluid flows through the channel and passes over the heated sections of the channel and finally exits the channel through the outlet.

The top wall of the channel is made of acrylic PMMA. A layer of micro capsulated phase change material (with the fusion temperature of 34.7 °C and the latent heat of 243 kJ/kg) is embedded inside the top wall. The phase change layer is filled with microencapsulated phase change material particles, and the pores are filled with air. The phase change layer absorbs some of the heat flux of the elements through the thermal conductive walls, and it also interacts with the working fluid through convective heat transfer. The thermophysical properties of materials are reported in Table 1 [27, 28].

2.1. Mathematical model

To mathematically model the flow and heat transfer in the microchannel, some basic assumptions are required. These basic assumptions are as follows: the nanoparticles are dispersed in the base fluid uniformly and the nanofluid is stable. Hence, no aggregation, sedition, or concentration gradient occurs in the nanofluid. In addition, there is no chemical reaction between the nanoparticles and the base fluid. The nanoparticles and the base fluid are in local thermal equilibrium due to very small size of nanoparticles. The nanofluid flow is incompressible and laminar with Newtonian behaviour. The thermophysical properties of the solid wall, the nanofluid and MEPCM layer are constant. Considering the phase change microcapsule layer inside the top wall, the container filled with the phase change microcapsules is assumed as a uniform and isotropic material filled with air with the porosity of ε_{pcml}.

The cross-section of microchannel is very small, and hence, the Reynolds number is low. Thus, the laminar flow assumption for the microchannel is considered and the results are reported for the fluid flow with the Maximum Reynolds number of 2000. The natural convection effects inside the microchannel and in the MEPCM layer are neglected due to very small size of the channel, and change phase occurs at the melting temperature.

Table 1
The thermophysical properties of the phase change micro capsules.

Material	density (kg/m³)	Specific thermal capacity (kJ/kg•K)	Thermal conductivity (W/m•K)
MEPCM	800	2.21	0.19
Air	1.29	1.005	0.024
copper	8960	385	401
Al_2O_3	3600	765	25.08
acrylic PMMA[27, 28]	1.18	1421	0.190

As the fluid flow in the channel is fully developed and the thermophysical properties are constant, the velocity profiles in the channel would remain fully develop and constant. Hence, following the study of Lee and Garimella [29], the analytic velocity profile in a three-dimensional channel with a rectangular cross section can be evaluated as:

$$u_x(y^+,z^+) = -\frac{16}{\pi^3}\left(\frac{dp}{dx^+}\right)\frac{W_{ch}^+}{\mu_{bf}}\sum_{n=1,3...}^{\infty}\frac{(-1)^{(n-1)/2}}{n^3}\left(1-\frac{\cosh(n\pi y^+/W_{ch}^+)}{\cosh(n\pi H_{ch}^+/2/W_{ch}^+)}\right)\cos\left(\frac{n\pi z^+}{W_{ch}^+}\right) \tag{1a}$$

Using the velocity profile of Eq. (1a), the bulk velocity of the nanofluid in the channel can also be evaluated as [29]:

$$u_b = -\frac{1}{12}\left(\frac{dp}{dx^+}\right)\frac{{W_{ch}^+}^2}{\mu_{bf}}\left\{1-\frac{192}{\pi^5}\left(\frac{W_{ch}^+}{H_{ch}^+}\right)\sum_{n=1,3...}^{\infty}\frac{1}{n^5}\tanh\left[\frac{n\pi(H_{ch}^+/W_{ch}^+)}{2}\right]\right\} \tag{1b}$$

where u_x is the velocity in the flow direction, and u_b is the bulk (average) velocity in the channel. dp/dx^+ is the pressure drop along the channel. The governing equations for the energy conservation in the nanofluid inside the channel, the solid walls and MEPCM are written as:

Nanofluid in microchannel:

$$\frac{\partial T}{\partial t} + u_x^+\frac{\partial T}{\partial x^+} = \frac{k_{nf}}{\rho_{nf}c_{p,nf}}\left(\frac{\partial^2 T}{\partial x^{+2}} + \frac{\partial^2 T}{\partial y^{+2}} + \frac{\partial^2 T}{\partial z^{+2}}\right) \tag{2}$$

The solid walls:

$$\frac{\partial T}{\partial t} = \frac{k_{cw}}{\rho_{cw}c_{p,cw}}\left(\frac{\partial^2 T}{\partial x^{+2}} + \frac{\partial^2 T}{\partial y^{+2}} + \frac{\partial^2 T}{\partial z^{+2}}\right) \tag{3}$$

MEPCM layer [30, 31]:

$$\frac{\partial T}{\partial t} = \frac{k_{pcml}}{\rho_{pcml}c_{p,pcml}}\left(\frac{\partial^2 T}{\partial x^{+2}} + \frac{\partial^2 T}{\partial y^{+2}} + \frac{\partial^2 T}{\partial z^{+2}}\right) - (1-\varepsilon_{pcml})\rho_{pcml}\frac{h_{ls}}{c_{p,pcml}}\left(\frac{\partial \xi}{\partial t}\right) \tag{4}$$

where T, ξ and t denote the temperature, melt phase field, and time, respectively. The thermophysical properties of k, ρ and c_p indicate the thermal conductivity, density and specific heat capacity, respectively. The subscripts of *pcml, cw* and *nf* denote the PCM layer, channel walls, and nanofluid, respectively. Here, h_{ls} is the latent heat of the MEPCM layer. In Eq. (4), the term $\partial\xi/\partial t$ denotes the melting rate which can be defined as follows [30, 31]:

$$\frac{\partial \zeta}{\partial t} = \frac{A_{pcmp}U_{pcmp}}{\rho_{pcm}h_{ls}V_{pcmp}}(T - T_M) \tag{5}$$

where A and V denote the perimeter area and the volume of the microencapsulated particles, respectively. The subscript of *pcmp* indicates the microencapsulated particle. Here, T_M is the fusion temperature, and U is the overall thermal heat transfer coefficient. The overall thermal heat transfer coefficient is evaluated using the following relation [30]:

$$U_{pcmp} = \frac{Nu_{pcmp}k_{pcmp}}{d_{pcmp}^+} \tag{6}$$

where d^+ is the size of microencapsulated particle, and Nu is the Nusselt number of the microencapsulated particle. The micro capsule is placed in the quiescent air, and hence, $Nu_{pcmp} = 2.0$. This Nusselt number, $Nu = 2.0$ corresponds to the heat transfer of a heated sphere in a large amount of stagnant fluid. More details about the governing equations and physical model can be found in [30–32].

Based on the problem description, the corresponding boundary conditions for the microchannel can be introduced as:

$$Initial condition: \quad t = 0: T(x^+,y^+,z^+,0) = T(x^+,y^+,z^+) \tag{7a}$$

and for $t > 0$:

$$\text{Inlet}: T = T_{in} \text{ and Outlet}: \partial T/\partial n^+ = 0; \tag{7b}$$

$$\text{At the insulated walls surfaces}: \partial T/\partial n^+ = 0 \text{ where } n \text{ is the surface normal} \tag{7c}$$

$$\text{At the inner walls surfaces of the channel}: k_{nf}\left(\partial T/\partial n^+\right)_{nf} = k_{cw}\left(\partial T/\partial n^+\right)_{cw} \text{and } T_{nf} = T_{cw} \tag{7d}$$

$$\text{At the interface of two different walls}: k_{nf}\left(\partial T/\partial n^+\right)_{nf} = k_{cw}\left(\partial T/\partial n^+\right)_{cw} \text{and } T_{nf} = T_{cw} \tag{7e}$$

$$\text{At the interface of pcm layer and wall}: k_{pcml}\left(\partial T/\partial n^+\right)_{pcml} = k_{cw}\left(\partial T/\partial n^+\right)_{cw} \text{and } T_{pcml} = T_{cw} \tag{7f}$$

$$\text{At the surfaces subject to heat flux}: -k_{cw}\left(\partial T/\partial n^+\right)_{cw} = q''_h(t) \tag{7g}$$

where $q"_h(t)$ is introduced as:

$$q''_h(t) = \begin{cases} q''_{h,1}, -\infty < t \le 0 \\ (1+\gamma)q''_{h,1}, 0 < t \le P \\ q''_{h,1}, P < t \le \infty \end{cases} \tag{8}$$

The microchannel is symmetric at the plane of x-y at $z = 0$. Hence, in order to reduce the computational costs, the channel is modeled as a symmetric channel where at the symmetric plane the zero heat-flux boundary condition, of $\partial T/\partial n^+ = 0$, is employed.

2.3. Non-dimensional form of governing equations

Invoking the following non-dimensional parameters:

$$\theta = \frac{T - T_{b,in}}{\Delta T_{ref,bf}}, and\ u_x = \frac{u_x^+}{u_b^+} \tag{9a}$$

the governing equations along with their boundary conditions are transformed into their non-dimensional form. In Eq. (9), θ and u denote the dimensionless temperature and the dimensionless velocity, respectively. The reference temperature difference is also evaluated as:

$$\Delta T_{ref,bf} = \frac{[(q''_{h,1}A_{h,1}^+ + q''_{h,2}A_{h,2}^+)/(A_{h,1}^+ + A_{h,2}^+)]D_h^+}{k_{bf}} \tag{9b}$$

The dimensionless form of governing equations is obtained as:

Nanofluid:

$$\frac{D_h}{\mathrm{Re}_{bf}\mathrm{Pr}_{bf}}\frac{\partial \theta}{\partial Fo} + u_x\frac{\partial \theta}{\partial x} = \alpha_{nf/bf}^*\frac{D_h}{\mathrm{Re}_{bf}\mathrm{Pr}_{bf}}\left(\frac{\partial^2\theta}{\partial x^2} + \frac{\partial^2\theta}{\partial y^2} + \frac{\partial^2\theta}{\partial z^2}\right) \tag{10}$$

Solid walls:

$$\frac{\partial\theta}{\partial Fo}=\alpha^*_{cw/bf}\left(\frac{\partial^2\theta}{\partial x^2}+\frac{\partial^2\theta}{\partial y^2}+\frac{\partial^2\theta}{\partial z^2}\right) \tag{11}$$

MEPCM layer:

$$\frac{\partial\theta}{\partial Fo}=\alpha^*_{pcm/bf}\left(\frac{\partial^2\theta}{\partial x^2}+\frac{\partial^2\theta}{\partial y^2}+\frac{\partial^2\theta}{\partial z^2}\right)-(1-\varepsilon_{pcml})\rho^*_{pcm/bf}\frac{1}{Ste^*}\frac{\partial\xi}{\partial Fo} \tag{12}$$

where the dimensionless parameters are:

$$k^*_{nf/bf}=\frac{k_{nf}}{k_{bf}},\ k^*_{cw/bf}=\frac{k_{cw}}{k_{bf}}\ and\ k^*_{pcml/bf}=\frac{k_{pcml}}{k_{bf}} \tag{13a}$$

$$\alpha^*_{nf/bf}=k^*_{nf/bf}\frac{\rho_{bf}c_{p,bf}}{\rho_{nf}c_{p,nf}},\alpha^*_{cw/bf}=k^*_{cw/bf}\frac{\rho_{bf}c_{p,bf}}{\rho_{cw}c_{p,cw}}and\ \alpha^*_{pcml/bf}=k^*_{pcml/bf}\frac{\rho_{bf}c_{p,bf}}{\rho_{pcml}c_{p,pcml}} \tag{13b}$$

and the non-dimensional numbers of Prandtl number (*Pr*), the Reynolds number (*Re*), Peclet number (*Pe*), Stefan number (Ste) are defined as:

$$\mathrm{Re}_{bf}=\frac{\rho_{bf}u^+_bD^+_h}{\mu_{bf}},\mathrm{Pr}_{bf}=\frac{\mu_{bf}}{\rho_{bf}\alpha_{bf}},Pe_{bf}=\frac{u^+_bD^+_h}{\alpha_{bf}} \tag{14a}$$

$$Ste_{pcml}=\frac{c_{p,pcml}\Delta T_{ref,bf}}{h_{ls}},\ Ste_{bf,ss}=\frac{c_{p,bf}\Delta T_{ref,bf}}{h_{ls}},\ Sb_{bf,in}=\frac{T_M-T_{b,in}}{\Delta T_{ref,bf}} \tag{14b}$$

where $\alpha_{bf}=k_{bf}/\rho\ c_p$, and the hydraulic diameter is evaluated as $D^+_h=\frac{2H^+_{ch}W^+_{ch}}{(H^+_{ch}+W^+_{ch})}=\frac{2AR_{ch,x}}{1+AR_{ch,x}}W^+_{ch}$.

The non-dimensional initial and boundary conditions are also obtained as:

$$\text{Initial condition}:\ t=0:\theta(x,y,z,0)=\theta(x,y,z) \tag{15a}$$

and for $t>0$:

$$\text{Inlet}:\theta=\theta_{in}\quad\text{and}\quad\text{Outlet}:\ \partial\theta/\partial n=0; \tag{15b}$$

$$\text{At the insulated walls surfaces}:\ \partial\theta/\partial n=0 \tag{15c}$$

$$\text{At the inner walls surfaces of the channel}:\ k^*{}_{nf/bf}(\partial\theta/\partial n)_{nf}=k^*{}_{cw/bf}(\partial\theta/\partial n)_{cw}\text{and}\,\theta_{nf}=\theta_{cw} \tag{15d}$$

$$\text{At the interface of two different walls}:\ k^*{}_{nf/bf}(\partial\theta/\partial n)_{nf}=k^*{}_{cw/bf}(\partial\theta/\partial n)_{cw}\text{and}\,\theta_{nf}=\theta_{cw} \tag{15e}$$

$$\text{At the interface of pcm layer and wall}:\ k^*{}_{pcml/bf}(\partial\theta/\partial n)_{pcml}=k^*{}_{cw.bf}(\partial\theta/\partial n)_{cw}\text{and}\,\theta_{pcml}=\theta_{cw} \tag{15f}$$

$$\text{At the surfaces subject to heat flux}:\ (\partial\theta/\partial n)_{cw}=q^{*\prime\prime}{}_h(t) \tag{15g}$$

where $q^{*\prime\prime}{}_h(t)$ is introduced as:

$$q^{*\prime\prime}_h(t)=\begin{cases}-1,\ -\infty<t\le 0\\ -\frac{k^*_{\mathrm{nf}/bf}}{k^*_{cw/bf}}(1+\gamma),0<t\le P\\ 1,\ P<t\le\infty\end{cases} \tag{16}$$

The thermophysical properties of MEPCM layer are evaluated using the following relations:

$$\rho_{pcml}=\phi_{pcml}\rho_{air}+(1-\phi_{pcml})\rho_{pcmp} \tag{17a}$$

$$c_{p,pcml}=\frac{\varepsilon_{pcml}\rho_{air}c_{p,air}+(1-\varepsilon_{pcml,f})\rho_{pcmp}c_{p,pcmp}}{\varepsilon_{pcml}\rho_{air}+(1-\varepsilon_{pcml})\rho_{pcmp}} \tag{17b}$$

where subscript of *air* denotes the air in MEPCM layer. The top phase change microcapsule layer is filled with 40% air and 60% micro capsules

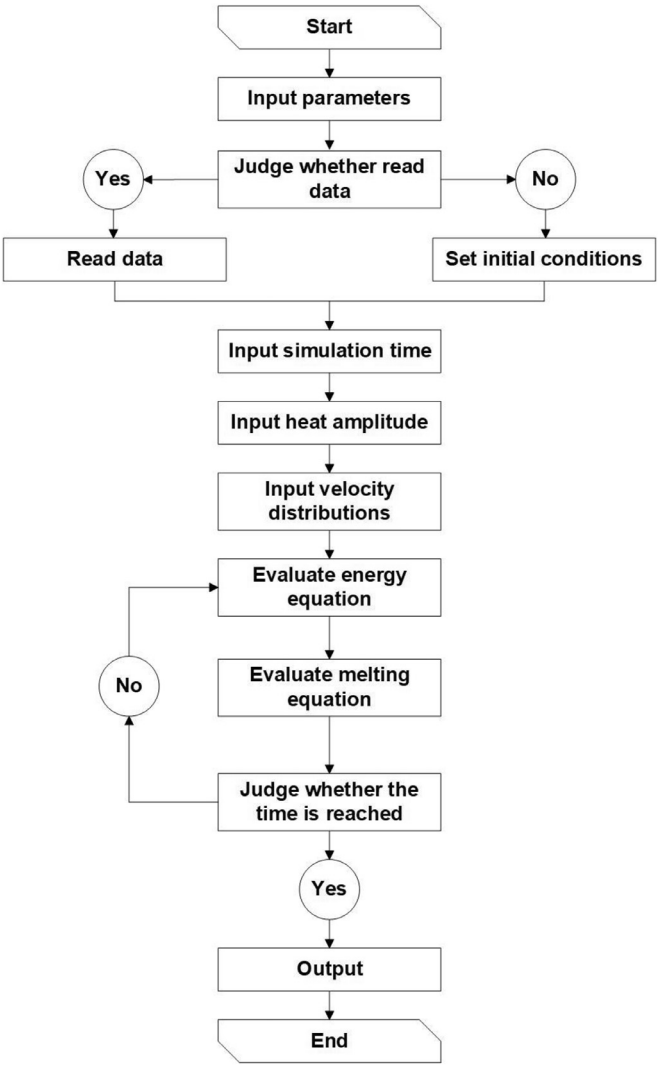

Fig. 2. The flowchart of the solution method.

which results in the porosity of MEPCM as $\varepsilon_{pcml}=0.4$. The thermophysical properties of the nanofluid are evaluated using the relations introduced in the study of Khanafer and Vafai [13] for nanoparticle of size 22.2~47.7 nm. In this work, two volume fractions (mass fractions) of $\phi=1.4\%$ ($\omega_{np}=5\%$) and $\phi=2.7\%$ ($\omega_{np}=10\%$) are studied. The important flow and heat transfer characteristics are defined as:

$$u^+_{b,x}(x^+)=\frac{1}{A^+_{ch,x}(=H^+_{ch}W^+_{ch})}\int_{y^+=0}^{H^+_{ch}}\int_{z^+=-W^+_{ch}/2}^{W^+_{ch}/2}u^+_x dy^+dz^+ \tag{18a}$$

$$\mathbf{T}_{b,x}=\frac{1}{\dot{Q}c_{p,m,0}}\int_{A^+_{ch,x}}c_{p,m}u^+_xTdA^+_{ch,x} \tag{18b}$$

$$\theta_{b,x}=\frac{T_b(x^+)-T_{b,in}}{\Delta T_{ref,bf}} \tag{18c}$$

where $u^+{}_{b,x}$, $T_{b,x}$ and $\theta_{b,x}$ are the bulk velocity, bulk temperature and non-dimensional bulk temperature. Here, $\dot{Q}(=u^+_{x,b}A^+_{ch,x})$ is the channel flow rate.

3. Numerical method

In the present study, the fluid flow was handled using the analytical solution. The melting rate equation is iteratively calculated by the transient method simulation. The system of discretized equations are solved numerically. Fig. 2 demonstrates the flowchart of the solution.

Table 2
The details of the utilized of grid tests.

Label	Grid numbers in heated section	Structure grid in heated section (long, wide, high)	Grid size in solid and PCM layer(height, width)	$T_{h,1,\max}$	error%
Grid1	254541	(161, 51, 31)	(41, 31)	80.8	0.30
Grid2	304451	(161, 61, 31)	(41, 31)	80.63	0.087
Grid3	468671	(161, 71, 31)	(41, 31)	80.56	X

The solution area can be divided into a base/side/top wall solid zone, a micro-channel fluid zone, and the MEPCM layer solid zone. The three parts of the solution area are solved in the order from the inlet section to the outlet. The longitudinal iterations are solved from the bottom to the top and then along the flow direction to the outlet. The boundary conditions at the acrylic and the layer of phase change microcapsule interfaces for temperature continuity and heat balance are simultaneously monitored and satisfied.

3.1. Grid check

The effect of grid size on the numerical results is analyzed by calculating the results for three different grid sizes. The details of the utilized grids are reported in Table 2. This table also shows the evaluated maximum steady state temperature, and the relative temperature calculation errors at the first heated zone for $Re_{bf}=500$. In Table 2, the results are evaluated for $q"_{h,1}=q"_{h,2}=29.6$ (W/cm^2), $T_{b,in}=34$ °C, $AR_{ch,x}=0.25$, $AR_{bw,x}=0.5$, $AR_{cw,c}=0.5$, $W_{sw}=1$. These parameters are also selected as the default values for calculation of future results in the present work, otherwise the value of each parameter will be stated. In the present study, it is also assumed that $q"_{h,1}=q"_{h,2}=q"_h$. The *error* in the Table 2 is the percentage of the relative error which calculated as 100 × (the difference of $T_{h,1}$ at the studied grid size - $T_{h,1,\max}$ at the grid size 3)/ $T_{h,1,\max}$ at the grid size 3. It is clear from Table 2 that the relative temperature error for Grid 2 is 0.087% which is suitable for most engineering calculations and the purpose of this study. Similarly, the relative temperature error at $Re_{bf}=2000$ is also evaluated which was 0.012% for Grid 2. Hence, Grid 2 is selected for future calculations.

The inlet section and the outlet section of the channel are also tested to be long enough to not affect the results. In fact, when the Reynolds number is high, the longer outlet section is required to capture the axial downstream thermal effects in channel walls and nanofluid flow. However, in the low Reynolds numbers in which the flow is slow, the axial conduction heat transfer effects toward upstream get important, and hence, a longer inlet section is required. After checking various sizes of inlet and outlet sections, it is found that the inlet section of $L^+_u/L^+=2$ and outlet section of $L^+_d/L^+=3$ are sufficient for the Reynolds number in the range of 500–2000.

3.2. Validation

To check the correctness and accuracy of the results, the results of the present study are compared with the results of heat transfer in a simple rectangular channel as reported by Lee and Garimella [29]. Using the present numerical approach, the same problem as those reported by Lee and Garimella is solved and the results are compared with the Nusselt number that is evaluated using the analytic solution in [29]. The results are plotted in Fig. 3. As seen, the results of the present study are in good agreement with the results available in the literature. In the separate numerical runs, the predicted Nusselt number is also compared with the previous work of Lee el al. [33]. It is found that the predicted Nusselt number is in agreement with the result of Lee et al. [33]. Thus, this result confirms the validity of the computational scheme used in the present investigation.

4. Results and discussion

The effects of the presence/absence of MEPCM on the transient temperature distribution of the channel system are studied. The calculations

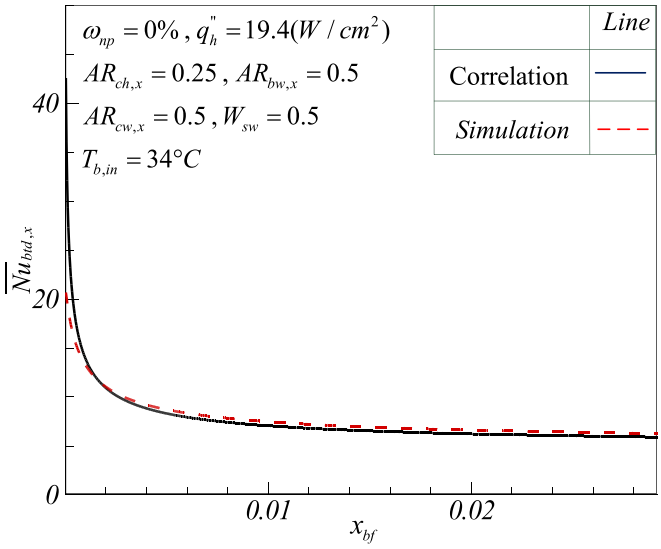

Fig. 3. A comparison between the Nusselt numbers evaluated in the present study and those reported in the study of Lee and Garimella [29].

Table 3
The maximum allowable temperature (°C) for various Reynolds numbers and various heat flux powers.

Heat flux	$Re_{bf}=500$	$Re_{bf}=2000$
$Ste^*_{bf,ss}=0.1$	56	–
$Ste^*_{bf,ss}=0.2$	75	60
$Ste^*_{bf,ss}=0.3$	92	72
$Ste^*_{bf,ss}=0.4$	–	82

are performed for the surface heat flux with normal heat flux until a steady solution is achieved ($t=0$ s). After two minutes (120 s) of steady state normal flux, a heating pulse of γ is suddenly applied at the heated zones to increase the heat flux. The results are evaluated for various heat flux powers. The heat flux powers of $q"_h=7.1$, 13.5, 16.5, 19.4 and 24.7 (W/cm^2) correspond to dimensional parameters of $Ste^*_{bf,ss}=0.1$, 0.2, 0.25, 0.3 and 0.4, respectively. Here, the heating pulse size is selected based on the maximum allowable heating power under different Reynolds numbers. These maximum temperatures for various Reynolds numbers and heat flux powers are summarized in Table 3. The pulse duration in the present study is adopted as 10 min, i.e. $P=10$ min (t = 121s-720 s) while the original heating power is 40 minutes. Hence, the total time for one cycle is 50 minutes.

In the present study, the main attention is on the cooling behaviour of the channel in the presence of the pulse heat flux. Hence, we have only reported the results for the temperature behaviour of the fluid and the heated locations. Furthermore, due to negligible effect of convective heat transfer in the very tiny layer of MEPCM, the temperature distribution in the molten part of MEPCM layer is linear and in the solid part is constant.

4.1. Bulk temperature distribution

The bulk temperature distributions along the flow direction during a heating cycle for Reynolds numbers of 500, 1000 and 2000, respectively, are shown in Figs. 4–6. The results are plotted for three sections of the channel. The first section is placed at the beginning of the first

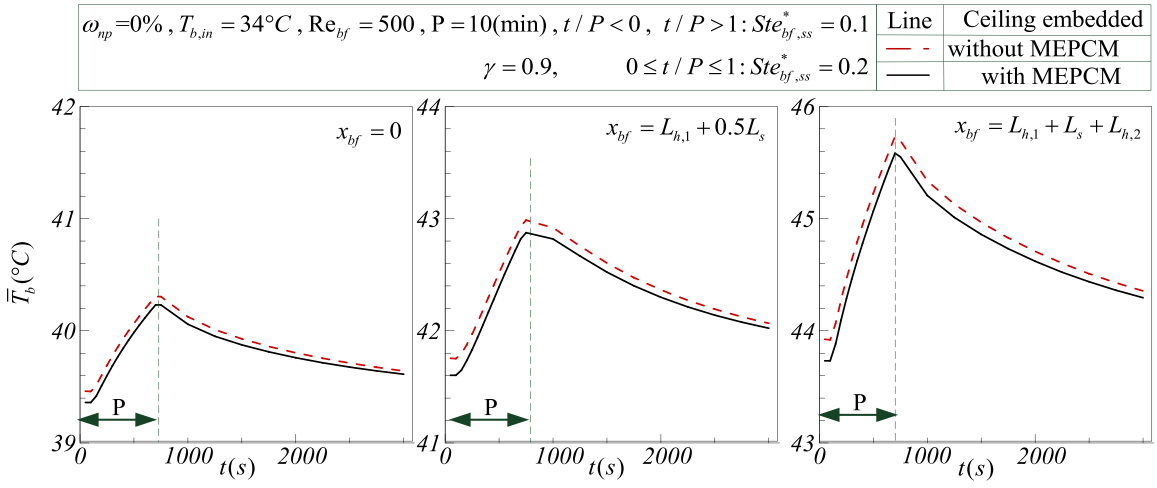

Fig. 4. The bulk temperature distribution at different locations with/without MEPCM during one cycle $Re_{bf}=500$, $\gamma=0.9$.

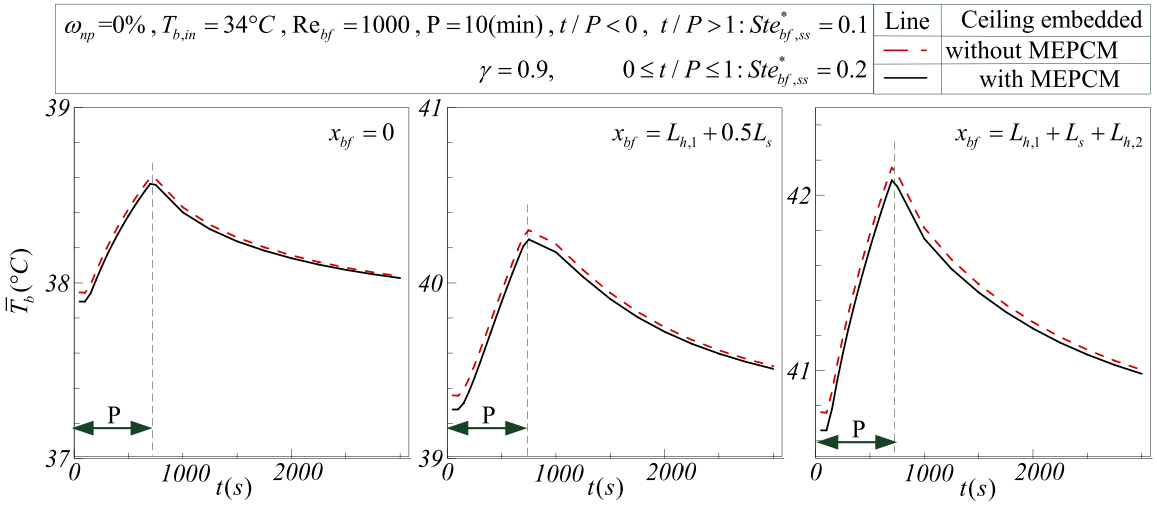

Fig. 5. The bulk temperature distribution at different locations with/without MEPCM during one cycle and $Re_{bf}=1000$, $\gamma=0.9$.

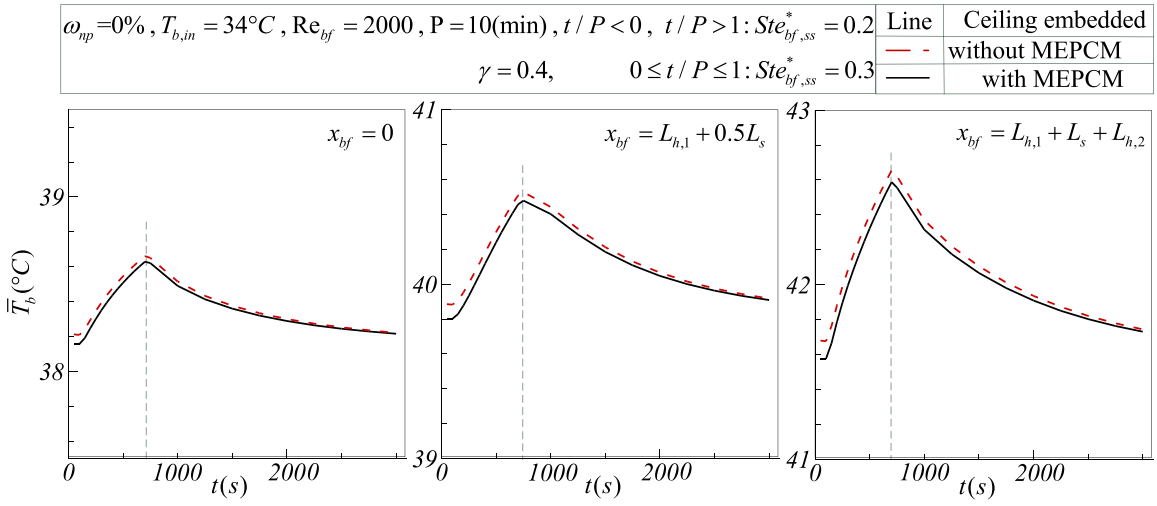

Fig. 6. The bulk temperature distribution at different locations with/without MEPCM during one cycle and $Re_{bf}=2000$, $\gamma=0.4$.

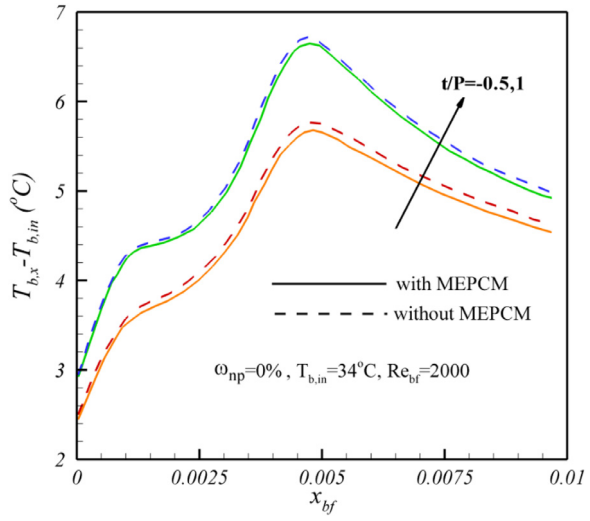

Fig. 7. The bulk temperature difference along the channel in flow direction with/without MEPCM for various times during one cycle and $Re_{bf}=2000$, $\gamma=0.4$.

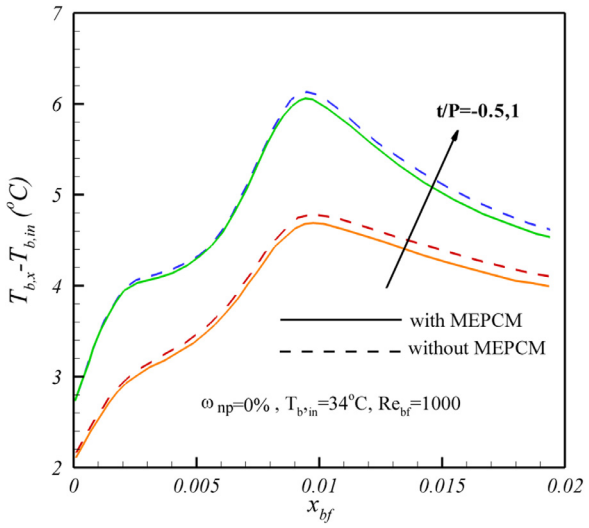

Fig. 8. The bulk temperature difference along the channel in flow direction with/without MEPCM for various times during one cycle and $Re_{bf}=1000$, $\gamma=0.9$.

heating zone, i.e. $x_{bf}=0$. The second section is located in the middle of the distance between two heated zones, i.e. $x_{bf}=L_{h,1}+0.5L_s$. The third section is after the second element, i.e. $x_{bf}=L_{h,1}+L_s+L_{h,2}$. The results are compared for two cases of the presence of MEPCM at the ceiling wall (top) wall and in the absence of MEPCM when $\omega_{np}=0\%$ (pure water). Fig. 4 clearly shows that the presence of the heat pulse rises the bulk temperature of the working fluid during its active time. The maximum temperature can be observed at the end of the pulse duration. As seen, the pulse heat flux induces a temperature raise about 2 °C after the second element. However, as depicted in Fig. 5, this temperature raise is as lows as 1 °C in the case of a higher Reynolds number, i.e. $Re_{bf}=1000$.

The results show that the temperature difference due to the presence of the MEPCM layer is more obvious in the case of low Reynolds numbers ($Re_{bf}=500$). In this case, the maximum temperature difference is 0.2 °C. The increase of Reynolds number diminishes the effect of the presence of the MEPCM layer. In the case of $Re_{bf}=1000$, the maximum temperature difference due to presence of the MEPCM layer is only 0.1 °C. Fig. 6 shows the results for lower amplitude of heat flux pulse of $\gamma=0.4$. As seen, the temperature differences are also smaller.

4.2. Bulk temperature difference in fluid flow

The bulk temperature differences (the difference between inlet and the fluid in the channel) along the channel in the flow direction for various time step ratios t/P are presented in Figs. 7–10. The results of Figs. 7 and 8 are plotted for two pulse flux amplitudes of $\gamma=0.4$ and $\gamma=0.9$. Here, $T_{b,in}$ and $T_{b,x}$ denote the bulk temperature of the fluid at inlet and the bulk temperature of the fluid at each channel cross-section, respectively. Figs. 7 and 8 aim to study the effect of the presence of the MEPCM layer on the bulk temperature raise of the channel. Figs. 9 and 10 denote the effect of various time steps in the range of $-0.5<t/P<5.0$. The negative time step of $t/P=-0.5$ denotes the steady state situation before the rise of the heat flux power. These figures show that the trend of the behaviour of the results in the presence or absence of the MEPCM layer is similar. This is because of the fact that the convective interaction between the MEPCM layer and the fluid is very low compared to conduction mechanism heat transfer with side walls. The most impact of the presence of MEPCM layer can be seen through conduction in side walls.

4.2. Average temperature of the channel walls

Figs. 11 and 12 are plotted to show the average temperature of the top wall of the channel in the presence or absence of the MEPCM layer and for two pulse powers of $\gamma=0.9$ and 1.30. The results of these figures are reported for various mass fractions of nanoparticles. These figures reveal the significant effect of the presence of MEPCM layer on the temperature of the top wall. The presence of nanoparticles smoothly affects the results. For lower sudden pulse power ($\gamma=0.9$), the wall temperature distributions for the cases without MEPCM are shown in red lines. It is clear in Fig. 11 that the maximum steady wall temperature is about 40.15 °C in the absence of the PCM layer. However, due to the lower thermal conductivity and density of MEPCM, the maximum steady wall temperature may be as high as 41.0 °C. So that, the MEPCM does not play an important role to reduce wall temperature raise for the case with a steady state situation or low sudden pulse power ($\gamma=0.9$). For high sudden pulse power ($\gamma=1.3$), i.e. Fig.12, the top wall with MEPCM has a role to reduce the wall temperature raise owing to the phase change effect.

Fig. 13 shows the temperatures difference between the bottom wall temperature and the inlet temperature for various mass fractions of nanoparticles. The pulse heat flux increases the temperature of the bottom wall. However, the presence of the MEPCM layer tends to absorb some of the heat, and hence, it smoothly decreases the maximum temperature of the bottom wall. The presence of the nanoparticles also smoothly affects the temperatures difference between the bottom wall and the bulk temperature of the working fluid. Although the results of the present study show little enhancement of heat transfer due to the presence of nanoparticles, the addition of the nanoparticles also increases the pressure drop in the channel due to the increase of dynamic viscosity. The increase of pressure drop requires more pumping power and is not of interest.

4. Conclusion

The heat transfer of Al_2O_3 nanofluids in a microchannel of rectangular cross-section with thick highly thermal conductive walls is modeled. A layer of microencapsulated PCM is embedded in the celling wall of the channel. The bottom wall of the channel is subject to two heat flux zones with pulse shape heat power. When the heat flux power increases, the MEPCM layer goes through a phase change process to absorb some of the extra heat fluxes of the heat flux pulse. The governing equations for heat transfer in the working nanofluid, the channel walls, and MEPCM layer are presented in the form of partial differential equations, and then, they transformed into non-dimensional form. The finite volume method is employed to solve the governing equations associated with the boundary conditions of the model. The results are compared with the literature results and found in good agreement. The results of the

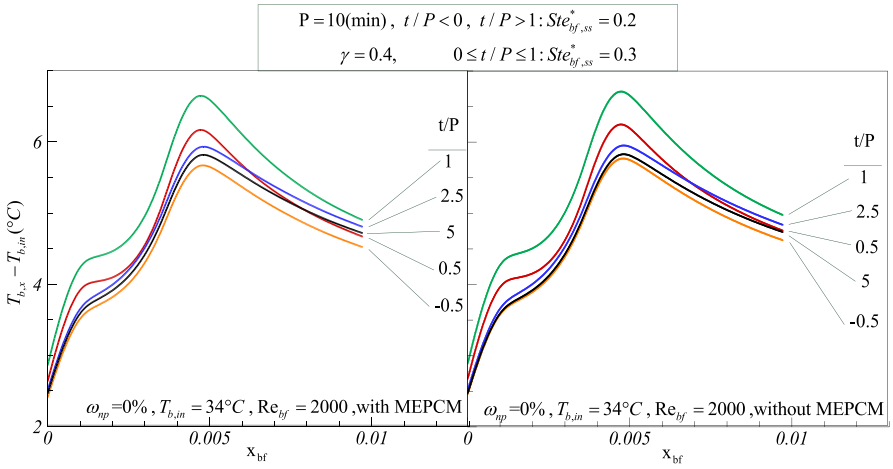

Fig. 9. The bulk temperatures difference along the channel in flow direction with/without MEPCM for various times during one cycle and $Re_{bf} = 2000$, $\gamma = 0.4$.

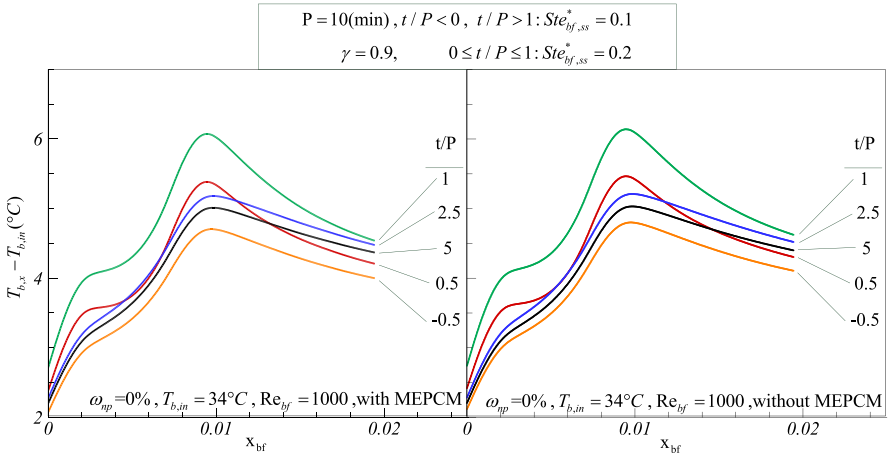

Fig. 10. The bulk temperatures difference along the channel in flow direction with/without MEPCM for various times during one cycle and $Re_{bf} = 1000$, $\gamma = 0.9$.

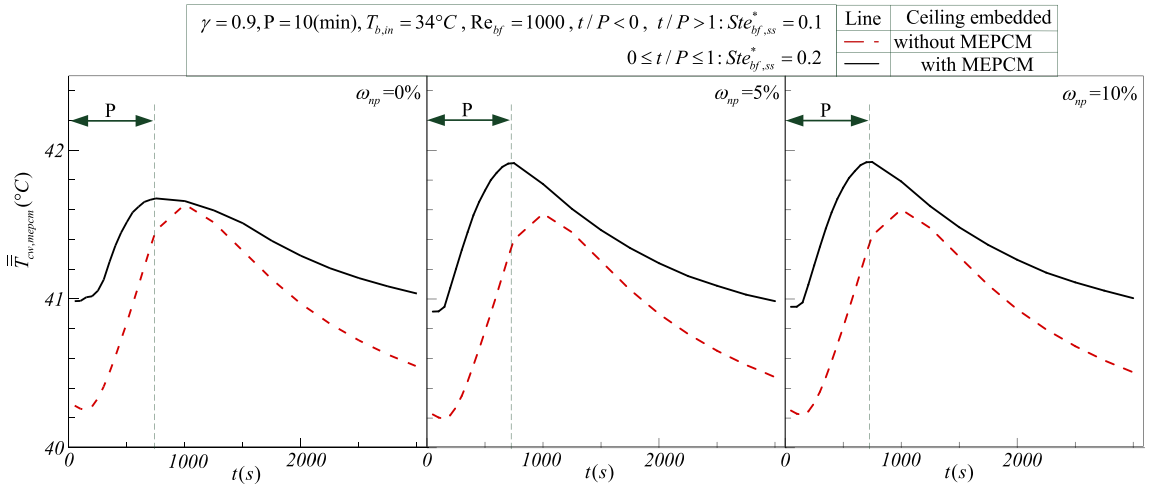

Fig. 11. The average temperature at celling wall of the channel with/without MEPCM for various mass fractions of nanoparticles during one cycle and $Re_{bf} = 1000$, $\gamma = 0.9$.

numerical calculations are reported in the form of plots and tables. The main outcomes of the present study can be summarized as follows:

1 The pulse heat flux rises the bulk temperature of the channel up to 2 °C. However, the average maximum temperature-difference of the fluid in the presence/absence of MEPCM is about 0.2 °C at low Reynolds number ($Re_{bf} = 500$). The average temperature difference of fluid caused by the presence/absence of MEPCM layer is about 0.1 °C for higher Reynolds numbers. The cooling effect the presence of MEPCM layer on lowering fluid temperature was not as expected. The heating pulse starts to increase the temperature very quickly until the temperature reaches to its highest value at the end of the heating pulse. After that, the temperature drops slowly under normal

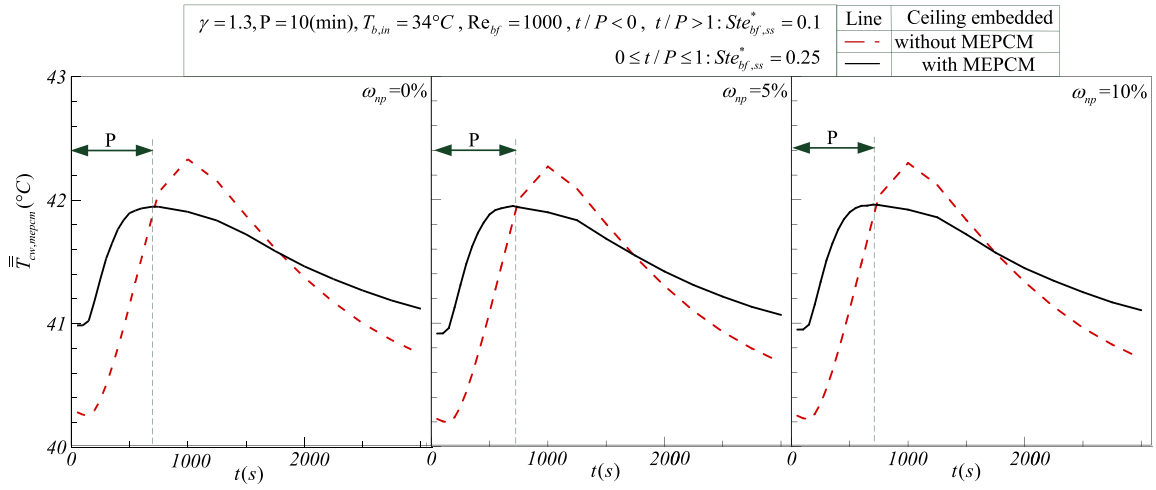

Fig. 12. The average temperature at celling wall of the channel with/without MEPCM for various mass fractions of nanoparticles during one cycle and $Re_{bf} = 1000$, $\gamma = 1.3$.

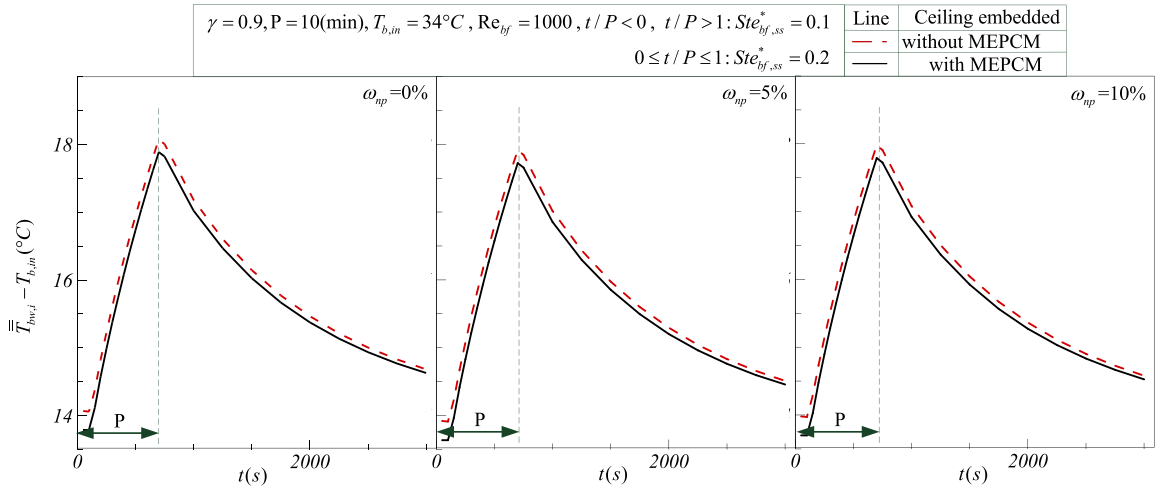

Fig. 13. The temperatures difference at interface of the bottom wall surface and nanofluid with/without MEPCM for various mass fractions of nanoparticles during one cycle and $Re_{bf} = 1000$, $\gamma = 0.9$.

heat flux condition, which is due to the axial heat transfer effects in the conductive walls of the channel.

2 The temperature of the celling wall is under influence of the MEPCM layer. It is found that the larger the amplitude of the heat flux pulse, the better cooling effect of the MEPCM layer. However, in the steady state case, the presence of the MEPCM layer can act as a barrier for heat transfer which is not of interest.

3 The presence of nanoparticles marginally enhances the heat transfer. The increase of the mass fraction of nanoparticles also improves the heat transfer enhancement.

In the present study, the effect of the presence of a MEPCM layer in the celling wall of the channel is studied. The results show that the interaction between the fluid and the MEPCM layer is low, and the MEPCM layer only would absorb some of the energy of the heat flux pulse due to conduction in the channel walls.

In the present study, the layer of MEPCM is considered at the celling section of the channel due to the low thermal conductivity of the MEPCM materials. Indeed, a large amount of heat exchange occurs between the bottom wall and the fluid inside the channel. This heat transfer mechanism is critically important to take away the off-pick heat of the heat sources. The side walls also partially contribute to the convective heat transfer with the fluid inside the channel through the conduction mechanism with the bottom wall. As a result, adding a low conductive layer to this part may significantly reduce the heat transfer rate. The celling is the part of the channel with minimum contribution in convection mechanism with the fluid flow. Thus, this part of the channel was supported using a layer of MEPCM to enhance the pick-load heat transfer using the phase change materials.

Another important point is the solidification of MEPCM. Usually, there is a significant difference between the solidification time and melting time of a PCM due to the difference between the mechanisms of natural convection and change in thermo-physical properties of the solid and liquid states. Considering the very thin layer of MEPCM, the natural convection effects are negligible. However, the change in the thermophysical conditions and the heat pathways of conjugate heat transfer inside the walls may be important. Study of the solidification of MEPCM layer in the channel can be the subject of future studies.

Acknowledgements

This study was partially supported by the Ministry of Science and Technology, Taiwan. The authors also acknowledge the financial support by the “Research Center of Energy Conservation for New Generation of Residential, Commercial, and Industrial Sectors” from The Featured Areas Research Center Program within the framework of the

Higher Education Sprout Project by the Ministry of Education (MOE) in Taiwan.

References

[1] K. Vafai, L. Zhu, Multi-layered micro-channel heat sink, devices and systems incorporating same. U.S. Patent 6675875B1, 2004.
[2] Leng C, Wang XD, Yan WM, Wang TH. Heat transfer enhancement of micro-channel heat sink using transcritical carbon dioxide as the coolant. Energy Convers Manage 2016;110:154–64.
[3] Ho CJ, Chang PC, Yan WM, Amani M. Comparative study on thermal performance of MEPCM suspensions in parallel and divergent minichannel heat sinks. Int Commun Heat Mass Transfer 2018;94:96–105.
[4] K. Vafai, L. Zhu, Two-layered micro channel heat sink, devices and systems incorporating same, U.S. Patent 6457515B1, 2002.
[5] Benzenine H, Saim R, Abboudi S, Imine O, Oztop HF, Abu-Hamdeh N. Numerical study of a three-dimensional forced laminar flow in a channel equipped with a perforated baffle. Numer Heat Transfer Part A 2018;73(12):881–94.
[6] Selimefendigil F, Öztop HF. Numerical analysis and ANFIS modeling for mixed convection of CNT-water nanofluid filled branching channel with an annulus and a rotating inner surface at the junction. Int J Heat Mass Transfer 2018;127:583–99.
[7] Selimefendigil F, Öztop HF. Magnetic field effects on the forced convection of CuO-water nanofluid flow in a channel with circular cylinders and thermal predictions using ANFIS. Int J Mech Sci 2018;146:9–24.
[8] Shirvan KM, Mamourian M, Mirzakhanlari S, Öztop HF, Abu-Hamdeh N, N. Numerical simulation and sensitivity analysis of effective parameters on heat transfer and homogeneity of Al2O3 nanofluid in a channel using DPM and RSM. Adv Powder Technol 2016;27(5):1980–91.
[9] Devendiran DK, Amirtham VA. A review on preparation, characterization, properties and applications of nanofluids. Renewable Sustainable Energy Rev 2016;60:21–40.
[10] Saidur R, Leong KY, Mohammad H. A review on applications and challenges of nanofluids. Renewable Sustainable Energy Rev 2011;15:1646–68.
[11] Khanafer K, Vafai K. A review on the applications of nanofluids in solar energy field. Renewable Energy 2018;123:398–406.
[12] Lee J, Mudawar I. Assessment of the effectiveness of nanofluids for single-phase and two-phase heat transfer in micro-channels. Int J Heat Mass Transfer 2007;50:452–63.
[13] Khanafer K, Vafai K. A critical synthesis of thermophysical characteristics of nanofluids. Int J Heat Mass Transfer 2011;54:4410–28.
[14] Ho CJ, Chen WC, Yan WM, Amani M. Cooling performance of MEPCM suspensions for heat dissipation intensification in a minichannel heat sink. Int J Heat Mass Transfer 2018;115:43–9.
[15] Ho CJ, Chang PC, Yan WM, Amani P. Efficacy of divergent minichannels on cooling performance of heat sinks with water-based MEPCM suspensions. Int J Therm Sci 2018;130:333–46.
[16] Farid MM, Al-Hallaj S. Microchannel heat exchanger with micro-encapsulated phase change material for high flux cooling. Illinois Inst. of Technology; 2012. U.S. Patent 8109324.
[17] Junior JR, Oliveski RDC, Rocha LAO, Biserni C. Numerical investigation on phase change materials (PCM): the melting process of erythritol in spheres under different thermal conditions. Int J Mech Sci 2018;148:20–30.
[18] Bondareva NS, Sheremet MA. Flow and heat transfer evolution of PCM due to natural convection melting in a square cavity with a local heater. Int J Mech Sci 2017;134:610–19.
[19] Boukani NH, Dadvand A, Chamkha AJ. Melting of a Nano-enhanced Phase Change Material (NePCM) in partially-filled horizontal elliptical capsules with different aspect ratios. Int J Mech Sci 2018;149:164–77.
[20] Jourabian M, Farhadi M. Melting of nanoparticles-enhanced phase change material (NEPCM) in vertical semicircle enclosure: numerical study. J Mech Sci Technol 2015;29(9):3819–30.
[21] Ghalambaz M, Doostani A, Chamkha AJ, Ismael MA. Melting of nanoparticles-enhanced phase-change materials in an enclosure: effect of hybrid nanoparticles. Int J Mech Sci 2017;134:85–97.
[22] Micro channel phase change heat transfer device, 2014 Patent, No. CN203733777U
[23] Jamekhorshid A, Sadrameli SM, Farid M. A review of microencapsulation methods of phase change materials (PCMs) as a thermal energy storage (TES) medium. Renewable Sustainable Energy Rev 2014;31:531–42.
[24] Sabbah R, Kizilel R, Selman JR, Al-Hallaj S. Active (air-cooled) vs. passive (phase change material) thermal management of high power lithium-ion packs: limitation of temperature rise and uniformity of temperature distribution. J Power Sources 2008;182(2):630–8.
[25] Ping P, Peng R, Kong D, Chen G, Wen J. Investigation on thermal management performance of PCM-fin structure for Li-ion battery module in high-temperature environment. Energy ConversManage 2018;176:131–46.
[26] Samimi F, Babapoor A, Azizi M, Karimi G. Thermal management analysis of a Li-ion battery cell using phase change material loaded with carbon fibers. Energy 2016;96:355–71.
[27] Soldera A, Metatla N, Beaudoin A, Said S, Grohens Y. Heat capacities of both PMMA stereomers: comparison between atomistic simulation and experimental data. Polymer 2010;51(2010):2106–11.
[28] Assael MJ, Botsios S, Gialou K, Metaxa IN. Thermal conductivity of polymethyl methacrylate (PMMA) and borosilicate crown glass BK7. Int J Thermophys 2005;26:1595–605.
[29] Lee PS, Garimella SV. Thermally developing flow and heat transfer in rectangular micro-channels of different aspect ratios. Int J Heat Mass Transfer 2006;49:3060–7.
[30] Ho CJ. A continuum model for transport phenomena in convective flow of solid–liquid phase change material suspensions. Appl Math Modell 2005;29:805–17.
[31] Ho CJ, Lin JF, Chiu SY. Heat transfer of solid–liquid phase-change material suspensions in circular pipes: effects of wall conduction. Numer Heat Transfer Part A 2004;45:171–90.
[32] Ho CJ, Siao CR, Yan WM. Thermal energy storage characteristics in an enclosure packed with MEPCM particles: an experimental and numerical study,. Int J Heat Mass Transfer 2014;73:88–96.
[33] Lee PS, Garimella SV, Liu D. Investigation of heat transfer in rectangular microchannels. Int J Heat Mass Transfer 2005;48:1688–704.